Compensated Ferrimagnets with Colossal Spin Splitting in Organic Compounds

Taiki Kawamura,[1] Kazuyoshi Yoshimi,[2] Kenichiro Hashimoto,[3] Akito Kobayashi,[1] and Takahiro Misawa[2,*]
[1]Department of Physics, Nagoya University, Nagoya, Aichi 464-8602, Japan
[2]Institute for Solid State Physics, University of Tokyo, Kashiwa, Chiba 277-8581, Japan
[3]Department of Advanced Materials Science, University of Tokyo, Kashiwa, Chiba 277-8561, Japan

(Received 17 November 2023; accepted 27 February 2024; published 10 April 2024)

The study of the magnetic order has recently been invigorated by the discovery of exotic collinear antiferromagnets with time-reversal symmetry breaking. Examples include altermagnets and compensated ferrimagnets, which show spin splittings of the electronic band structures even at zero net magnetization, leading to several unique transport phenomena, notably spin-current generation. Altermagnets demonstrate anisotropic spin splitting, such as *d*-wave, in momentum space, whereas compensated ferrimagnets exhibit isotropic spin splitting. However, methods to realize compensated ferrimagnets are limited. Here, we demonstrate a method to realize a fully compensated ferrimagnet with isotropic spin splitting utilizing the dimer structures inherent in organic compounds. Moreover, based on *ab initio* calculations, we find that this compensated ferrimagnet can be realized in the recently discovered organic compound $(\mathrm{EDO\text{-}TTF\text{-}I})_2\mathrm{ClO}_4$. Our findings provide an unprecedented strategy for using the dimer degrees of freedom in organic compounds to realize fully compensated ferrimagnets with colossal spin splitting.

DOI: 10.1103/PhysRevLett.132.156502

Introduction.—Collinear antiferromagnets have traditionally been viewed as conventional magnetic orderings that lack unique phenomena such as spin-current generation. However, recent theoretical advances have identified exotic collinear antiferromagnets with time-reversal breaking, notably altermagnets [1–3] and compensated ferrimagnets [4]. These magnetic states exhibit spin splitting in their electronic band structures even without net magnetization. Because spin splitting may drive spin-dependent novel transport phenomena and unconventional superconducting phases, these distinctive antiferromagnets have attracted considerable attention.

Several materials have been proposed as candidates for altermagnetism [3,5–13]. For example, κ-ET-type organic compounds [6] and transition metal oxide RuO_2 [8,10,14] exhibit altermagnetism with anisotropic spin splitting in electronic band structures. These materials are expected to exhibit spin-dependent transport and anomalous Hall effects owing to anisotropic spin splitting. In contrast, compensated ferrimagnets offer isotropic spin splitting, increasing efficiency for spin-current generation. The concept of metallic compensated ferrimagnetism (half-metallic antiferromagnetism) was introduced by van Leuken and de Groot [15]. Since then, several candidate materials have been suggested using *ab initio* calculations [16,17]. More recently, monolayer MnF_2 was proposed as an insulating compensated ferrimagnet [18]. Since the magnetic moment of compensated insulating ferrimagnets is strictly zero due to the Luttinger theorem [4], small perturbations do not change the compensation condition. In addition, compensated ferrimagnets have lower crystal symmetry than altermagnets [4]. Therefore, compensated ferrimagnets have advantages over altermagnets, leading to various potential applications, such as thin-film synthesis. However, the number of compensated ferrimagnets discovered experimentally is limited [19–22]. To harness the compensated ferrimagnets, a simple method to realize them is necessary.

In this Letter, we present a path toward fully compensated ferrimagnets with colossal spin splitting using typical dimer structures in organic compounds. Using a simple one-dimensional model, we demonstrate that a collinear antiferromagnetic order with inequivalent dimers can induce fully compensated ferrimagnets. Furthermore, we find that the recently discovered organic compound $(\mathrm{EDO\text{-}TTF\text{-}I})_2\mathrm{ClO}_4$ [EDO-TTF-I = 4, 5-ethylenedioxy-4′-iodotetrathiafulvalene] [23] can realize this mechanism based on *ab initio* calculations. The experiments demonstrate that $(\mathrm{EDO\text{-}TTF\text{-}I})_2\mathrm{ClO}_4$ undergoes a structural transition with anionic ordering at 190 K. Below the structural transition, unit-cell doubling occurs with the extended unit cell containing two inequivalent dimers. By deriving and solving the *ab initio* effective Hamiltonian for the low-temperature phase of $(\mathrm{EDO\text{-}TTF\text{-}I})_2\mathrm{ClO}_4$, we find that the ground state is a collinear antiferromagnet with isotropic spin splitting, i.e., a fully compensated ferrimagnet.

Simple model.—First, to show the key idea for realizing the compensated ferrimagnets, we consider a one-dimensional model whose unit cell contains two

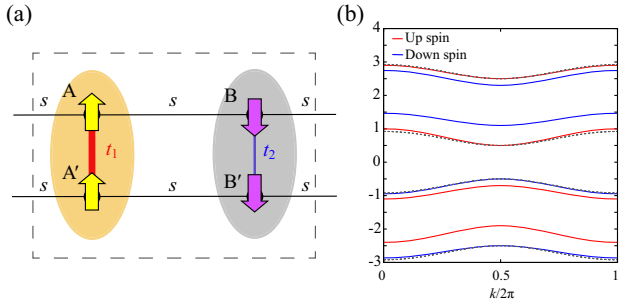

FIG. 1. (a) Schematic of a one-dimensional model showing the compensated ferrimagnetism. The broken lines show a unit cell. The interdimer hopping integral s and the intradimer hopping integrals t_1 and t_2 are represented by the horizontal thin black lines, the vertical thick red line, and the vertical thin blue line, respectively. The up (down) spin polarizations are described by the yellow upward (purple downward) arrows. (b) Band structures of the Hamiltonian defined in Eq. (2). We take $t_1 = 1.0$, $t_2 = 0.6$, $s = 0.6$, $\delta = 0.2$, and $\Delta = 1.5$. For comparison, we also show the band structures of the equivalent dimer case with the broken curves, whose parameters are given by $t_1 = t_2 = 1.0$, $s = 0.6$, $\delta = 0.0$, and $\Delta = 1.5$.

inequivalent dimers. A schematic of the model is illustrated in Fig. 1(a). The inequivalence between the two dimers is characterized using difference between the intradimer hoppings t_1 and t_2 and chemical potential difference δ. We also consider the collinear dimer antiferromagnetic (DAF) state, where the up-(down-)spin electrons are located on A and A′ (B and B′). This DAF state is not invariant to any combination of time reversal with translation or rotation operations because of dimer inequivalence. Thus, isotropic spin splitting is expected in this dimer collinear DAF state.

To determine the mechanism of spin splitting in this model, we consider the following tight-binding Hamiltonian for the DAF state:

$$\mathcal{H} = \sum_{k,\sigma} \boldsymbol{c}^{\dagger}_{k\sigma} H_{\sigma}(k) \boldsymbol{c}_{k\sigma}, \tag{1}$$

$$H_{\sigma}(k) = \begin{pmatrix} \sigma\Delta & t_1 & A(k) & 0 \\ t_1 & \sigma\Delta & 0 & A(k) \\ A(k)^* & 0 & -\sigma\Delta + \delta & t_2 \\ 0 & A(k)^* & t_2 & -\sigma\Delta + \delta \end{pmatrix}, \tag{2}$$

where $\boldsymbol{c}^{\dagger}_{k\sigma} = (c^{\dagger}_{Ak\sigma}, c^{\dagger}_{A'k\sigma}, c^{\dagger}_{Bk\sigma}, c^{\dagger}_{B'k\sigma})$, $A(k) = s(1 + e^{-ik})$ and Δ denotes the gap induced by the DAF order. The spin index σ takes $+1$ and -1 for the up and down spins, respectively. The eigenvalues of this Hamiltonian are given by

$$E_{0,\sigma,\pm}(k) = \delta/2 + t_+ \pm [(\sigma\Delta + t_- - \delta/2)^2 + 2s^2 C(k)]^{1/2}, \tag{3}$$

$$E_{1,\sigma,\pm}(k) = \delta/2 - t_+ \pm [(\sigma\Delta - t_- - \delta/2)^2 + 2s^2 C(k)]^{1/2}, \tag{4}$$

where $t_{\pm} = (t_1 \pm t_2)/2$ and $C(k) = (1 + \cos k)$. Thus, spin splitting of the bands is induced by $t_- = (t_1 - t_2)/2$ and δ, i.e., inequivalence of the dimers. From these expressions, it is evident that the differences in intradimer hoppings have the similar gap-opening effect as the differences in the chemical potentials. Because t_- and δ are independent of the wave number, spin splitting is isotropic.

Figure 1(b) shows the electronic band structures of the Hamiltonian defined in Eq. (2) for a typical parameter set. We also plot the band structures when the two dimers are equivalent ($t_1 = t_2$ and $\delta = 0$). As expected, isotropic spin splitting occurs in the band structures. At commensurate filling (i.e., three-quarter, half, and quarter filling), the DAF state is insulating, and the net magnetization is zero because the number of up and down bands below the Fermi energy are the same. Thus, the DAF state at the commensurate filling is the fully compensated ferrimagnets with isotropic spin splitting.

Crystal and electronic structures of $(\mathrm{EDO\text{-}TTF\text{-}I})_2\mathrm{ClO}_4$.—First, we summarize the crystal structure of $(\mathrm{EDO\text{-}TTF\text{-}I})_2\mathrm{ClO}_4$. $(\mathrm{EDO\text{-}TTF\text{-}I})_2\mathrm{ClO}_4$ consists of EDO-TTF-I molecule with $+1/2$ charge (3/4 filling) and anion ClO_4 layers. Above 190 K, the unit cell contains two EDO-TTF-I molecules and space inversion symmetry is macroscopically protected because of the random orientation of ClO_4. By lowering the temperature, the structural phase transition with anion ordering occurs at approximately $T = 190$ K, which induces unit-cell doubling, as evidenced by the x-ray analysis. As shown in Fig. 2(a), each unit cell contains four molecules in the low-temperature phase. A and A′ (B and B′) molecules in a unit cell form a dimer, referred to as dimer I (dimer II). The inversion centers are at the centers of each dimer. The inequivalence of the dimers I and II can also be understood from the partial densities of states, which are shown in the Supplemental Material [24]. Because dimers I and II are inequivalent after the structural phase transition, $(\mathrm{EDO\text{-}TTF\text{-}I})_2\mathrm{ClO}_4$ will exhibit compensated ferrimagnetism if appropriate antiferromagnetic order occurs. We note the related organic compound $(\mathrm{EDO\text{-}TTF\text{-}I})_2\mathrm{PF}_6$ [25] has similar crystal structures; however, all the dimers are equivalent. This indicates that the ordering of ClO_4 plays an essential role in realizing inequivalent dimers.

Next, we summarize the low-temperature electronic structure of $(\mathrm{EDO\text{-}TTF\text{-}I})_2\mathrm{ClO}_4$. Although the resistivity exhibits semimetallic behavior immediately after the structural phase transition, a metal-insulator phase transition occurs at approximately $T = 95$ K [23]. It is confirmed that the metal-insulator transition does not accompany a structural change. As explained later, *ab initio* analysis suggests

that the DAF ordering is the origin of the insulating phase although the origin of the metal-insulator transition is not experimentally clarified yet.

Ab initio effective Hamiltonian for $(EDO\text{-}TTF\text{-}I)_2ClO_4$.—To investigate the electronic structures of the low-temperature phase in $(EDO\text{-}TTF\text{-}I)_2ClO_4$, we derive the *ab initio* low-energy effective Hamiltonian, based on band structures obtained by the density functional theory (DFT). We use Quantum ESPRESSO [26] to obtain the DFT bands. In this study, we employ the optimized norm-conserving Vanderbilt pseudopotentials and plane-wave basis sets [36,37]. The exchange-correlation functional used in this study is the generalized gradient approximation proposed by Perdew, Burke, and Ernzerhof [38]. The cutoff energy of the wave functions and charge densities are set to be 80 and 320 Ry, respectively. During the self-consistent loop process, a $5 \times 5 \times 3$ uniform $\boldsymbol{k}$-point grid and Methfessel-Paxton smearing method are used [39]. We use the crystal structure data at 100 K [23]. We perform structural optimization for hydrogen atoms and use the optimized structure in the following analyses. In the DFT calculations, we only consider the paramagnetic solutions. Figure 2(b) shows the obtained energy band structures of $(EDO\text{-}TTF\text{-}I)_2ClO_4$. The four bands around the Fermi level, which are isolated from the other bands, mainly consist of the highest occupied molecular orbitals of the four EDO-TTF-I molecules in the unit cell (A, A′, B, and B′). We select these four bands as the low-energy degrees of freedom and use them to construct the maximally localized Wannier functions (MLWFs) using RESPACK [27]. Isosurfaces of the MLWFs are shown in Fig. 2(a). In addition, we confirm that the bands interpolated by the MLWFs accurately reproduce the DFT band structures [Fig. 2(b)].

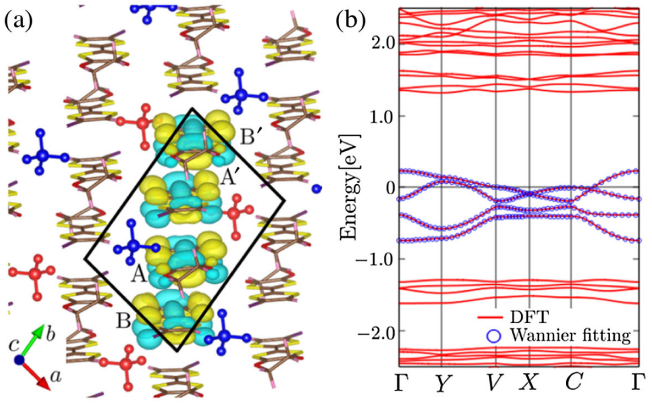

FIG. 2. (a) Crystal structure of $(EDO\text{-}TTF\text{-}I)_2ClO_4$ at $T = 100$ K and the real-space distribution of maximally localized Wannier functions (MLWFs) drawn by VESTA [35]. Anions ClO_4 are represented by balls and rods. Colors of anions represent their orientations. Because of the different configurations of anions around the dimers, two dimers (A-A′ and B-B′) become inequivalent. Black lines show the unit cell including four molecules. (b) Energy band structure obtained by the DFT calculation (red lines) and the MLWFs (blue circles) for the paramagnetic states. The Fermi energy is set to zero.

After constructing MLWFs, we derive a low-energy effective Hamiltonian, which is given by

$$\begin{aligned} H_{\mathrm{EDO}} &= H_0 + H_{\mathrm{int}}, \\ H_0 &= \sum_{i,j,\alpha,\beta,\sigma} t_{i\alpha j\beta} c^{\dagger}_{i\alpha\sigma} c_{j\beta\sigma}, \\ H_{\mathrm{int}} &= \sum_{i,\alpha} U_{i\alpha} n_{i\alpha\uparrow} n_{i\alpha\downarrow} + \frac{1}{2} \sum_{i,j,\alpha,\beta} V_{i\alpha j\beta} N_{i\alpha} N_{j\beta}, \end{aligned} \tag{5}$$

where $c^{\dagger}_{i\alpha\sigma}$ ($c_{i\alpha\sigma}$) is a creation (annihilation) operator for an electron in the ith unit cell with orbitals $\alpha = \mathrm{A}, \mathrm{A}', \mathrm{B}, \mathrm{B}'$, and spin σ. The number operators are defined as $n_{i\alpha\sigma} = c^{\dagger}_{i\alpha\sigma} c_{i\alpha\sigma}$ and $N_{i\alpha} = n_{i\alpha\uparrow} + n_{i\alpha\downarrow}$. The transfer integrals $t_{i\alpha j\beta}$ are evaluated using the MLWFs. We also evaluate the screened Coulomb interactions $U_{i\alpha}$ and $V_{i\alpha j\beta}$ using the constrained random phase approximation [40,41] implemented in RESPACK [27]. We set the cutoff energy of the polarization function to 5.0 Ry. Details of the transfer integrals and interaction parameters are summarized in the Supplemental Material [24]. We note that the difference in the intradimer hoppings t_1 and t_2 and the existence of the site potential δ indicate the inequivalence of the dimers. In actual calculations, we subtract a constant value Δ_{DDF} from on-site and off-site Coulomb interactions to consider the interlayer screening [28,29]. Following previous studies [29–32], we employ $\Delta_{\mathrm{DDF}} = 0.2$ eV. We confirm that the results are insensitive to Δ_{DDF}. We also perform an electron-hole transformation to reduce the numerical cost.

Many-variable variational Monte Carlo (mVMC) analysis.—The effective Hamiltonian is solved using the mVMC method [33,42], which can take into account quantum fluctuations and spatial correlations seriously. The trial wave function used in this study is given by

$$|\psi\rangle = \mathcal{P}_G \mathcal{P}_J \mathcal{L}_S |\phi_{\mathrm{pair}}\rangle, \tag{6}$$

$$\mathcal{P}_G = \exp\left[\sum_i g_i n_{i\uparrow} n_{i\downarrow}\right], \tag{7}$$

$$\mathcal{P}_J = \exp\left[\frac{1}{2}\sum_{i\neq j} v_{ij} N_i N_j\right], \tag{8}$$

$$|\phi_{\mathrm{pair}}\rangle = \left[\sum_{i,j}^{N_{\mathrm{site}}} f_{ij} c^{\dagger}_{i\uparrow} c^{\dagger}_{j\downarrow}\right]^{N_e/2} |0\rangle, \tag{9}$$

where $\mathcal{P}_G$, $\mathcal{P}_J$, and $\mathcal{L}_S$ are the Gutzwiller factor [43], long-range Jastrow factor [44,45], and total spin projector [46,47], respectively [33,48]. N_e and N_{site} indicate the number of electrons and sites, respectively. We impose a 1×4 sublattice structure on variational parameters. We use

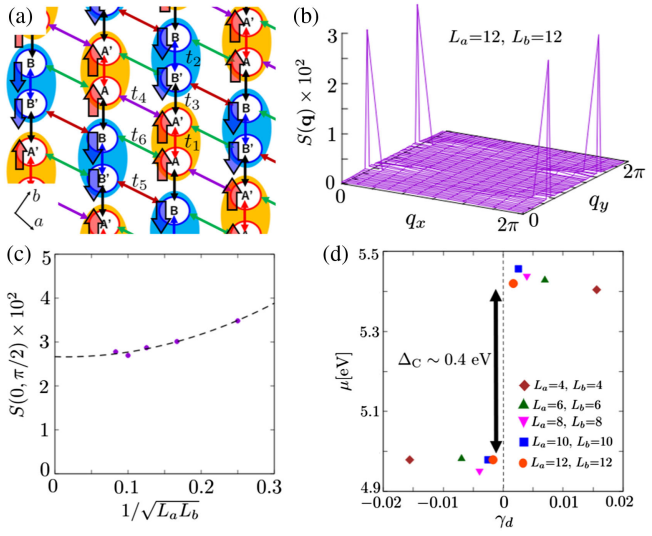

FIG. 3. (a) Schematic of the DAF state and representative hopping integrals (t_1–t_6) in the conducting layer of (EDO-TTF-I)$_2$ClO$_4$. (b) Spin structure factor obtained by the mVMC method for $L_a = L_b = 12$. Sharp peaks appear at $\boldsymbol{q} = (0, \pi/2), (0, 3\pi/2)$, which correspond to the DAF state. (c) Size dependence of the peak value of the spin structure factors. (d) Doping dependence of the chemical potential.

the Hartree-Fock approximation results as the initial f_{ij} values. The spin-singlet projection ($S = 0$) is used in ground-state calculations for $L_a = L_b \leq 8$, while it is not used for $L_a = L_b \geq 10$ to reduce the numerical costs. We confirm that the spin projection does not largely affect physical quantities, such as the spin structure factors. All variational parameters are simultaneously optimized using the stochastic reconfiguration method [49].

As detailed in the Supplemental Material, the Hartree-Fock approximation shows that the DAF state [Fig. 3(a)] and antiferromagnetic states with charge ordering (AF + CO) are ground-state candidates. Within the Hartree-Fock approximation, the ground state of the effective Hamiltonian is the AF + CO state. However, using the mVMC method, we find that the DAF state becomes the ground state of the effective Hamiltonian. We also find that the AF + CO state converges to the DAF state after optimization, even when using the variational parameters of AF + CO state as the initial state. This result indicates that correlation effects beyond the mean-field approximation are important in stabilizing the DAF state.

To examine the existence of long-range antiferromagnetic order, we calculate the spin-correlation functions of the ground state, defined as

$$S(\boldsymbol{q}) = \frac{1}{(N_{\text{site}})^2} \sum_{i,j} \langle \boldsymbol{S}_i \cdot \boldsymbol{S}_j \rangle e^{i\boldsymbol{q}\cdot(\boldsymbol{r}_i - \boldsymbol{r}_j)}, \tag{10}$$

where the original lattice structure is mapped to the equivalent $L_a \times 4L_b$ square lattice for simplicity. Figure 3(b) shows $S(\boldsymbol{q})$ in the momentum space, with sharp Bragg peaks at $(q_x, q_y) = (0, \pi/2)$ and $(0, 3\pi/2)$. As shown in Fig. 3(c), we confirm that the peak values of $S(\boldsymbol{q})$ remain finite in the thermodynamic limit. We also confirm that charge densities are uniform and there is no signature of a charge-ordered state. These results show that the ground state of the effective Hamiltonian is the DAF state. In addition, we calculate the charge gap Δ_c, given by $\Delta_c = \mu(N_e + 1) - \mu(N_e - 1)$, where the chemical potential is defined as $\mu(N_e + 1) = [E(N_e + 2) - E(N_e)]/2$. Figure 3(d) shows the doping rate $\gamma_d = N_e/N_{\text{site}} - 1.5$ dependence of the chemical potential. From this plot, we estimate the charge gap [$\Delta_c = \mu(N_e + 1) - \mu(N_e - 1)$] as $\Delta_c \sim 0.4$ eV. This result indicates that the ground state of (EDO-TTF-I)$_2$ClO$_4$ is the DAF insulator.

Spin splitting.—Based on the results obtained using the mVMC method, we analyze spin splitting in the DAF state using the Hartree-Fock approximation (for more details, see Ref. [24]). We assume the DAF order and scale the interaction parameters to reproduce the charge gap $\Delta_c \sim 0.4$ eV obtained from the mVMC calculations. The scaling ratio λ, which monotonically scales the on-site and off-site Coulomb interactions, is estimated to be $\lambda = 0.7$. The details of the Hartree-Fock calculations are provided in the Supplemental Material.

Using the Hartree-Fock approximation, we calculate the density of state (DOS) defined as $D_\sigma(\omega) = (\pi L_a L_b)^{-1} \sum_{\boldsymbol{k},n} \text{Im}(\omega - i\eta - E_{\boldsymbol{k},n,\sigma} + \mu)^{-1}$, where μ and η are the chemical potential and the smearing factor, respectively. $E_{\boldsymbol{k},n,\sigma}$ denotes the nth eigenvalue of the mean-field Hamiltonian at momentum $\boldsymbol{k}$. We set $\eta = 0.002$ eV. As shown in Fig. 4(a), spin splitting occurs in the DAF order [$D_\uparrow(\omega) \neq D_\downarrow(\omega)$]. The electronic band dispersions in Fig. 4(b) also show isotropic spin splitting over the entire Brillouin zone. This demonstrates that (EDO-TTF-I)$_2$ClO$_4$ can be fully compensated ferrimagnets if a DAF order occurs.

Here, we analyze the origin of spin splitting in (EDO-TTF-I)$_2$ClO$_4$. As in the case of the simple model,

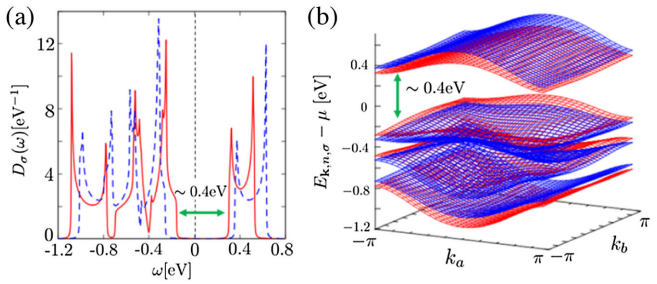

FIG. 4. (a) DOS of the low-energy effective Hamiltonian (EDO-TTF-I)$_2$ClO$_4$ for the DAF state obtained by the Hartree-Fock approximation. DOS for up (down) spin is described by the red (blue) lines. (b) Band dispersions of the DAF state obtained by the Hartree-Fock approximation. The red (blue) surfaces describe up-spin (down-spin) band dispersions.

$t_- = (t_1 - t_2)/2$ and δ can induce spin splitting. From the *ab initio* calculations, we find that $t_- = 0.036$ eV is comparable to $\delta = 0.047$ eV. Thus, spin splitting in $(\text{EDO-TTF-I})_2\text{ClO}_4$ is induced by both t_- and δ. One might think that finite δ would make the total magnetization finite; however, a charge gap guarantees that the total magnetization is robust against perturbations. In this case, the total magnetization is zero at $\delta = 0$ and remains zero even if δ is added, provided that δ is significantly smaller than the charge gap.

Summary and discussion.—In this Letter, we present a simple method to realize fully compensated ferrimagnetism using the dimer degrees of freedom, which are typical of organic compounds. Using a simple model, we demonstrate that the inequivalence of the two dimers and DAF order can induce fully compensated ferrimagnets at commensurate filling. Furthermore, *ab initio* calculations suggest that the ground state of $(\text{EDO-TTF-I})_2\text{ClO}_4$ is a DAF insulator with inequivalent dimers. As a result, the DAF order induces isotropic spin splitting in the electronic band structure. Our study shows that the key to realizing compensated ferrimagnetism lies in inequivalent dimer structures induced by anion ordering. This finding offers an unanticipated direction in materials design, where exotic magnetism can be achieved by selecting and modifying anions to exhibit anion ordering. The discovery of compensated ferrimagnetism in inequivalent dimer structures, as well as the potential for materials design using anion ordering, demonstrates that organic compounds offer a versatile platform for realizing exotic magnetism. An intriguing future issue would be to examine the doping effects in the DAF insulating state. Because the lowest unoccupied band is fully polarized and its DOS is large [Fig. 4(a)], unconventional superconductivity, such as triplet superconductivity, is expected [50]. Further experimental and theoretical investigations in this direction are desirable.

The authors thank Y. Nakano, M. Ishikawa, H. Yamochi, and A. Otsuka for the fruitful discussions. This work was financially supported by Grants-in-Aid for Scientific Research (KAKENHI) (Grants No. 23H03818, No. 23KJ1065, No. 15K05166, No. 22K18683, No. 22K03526, and No. 21H01793), Grant-in-Aid for Scientific Research for Transformative Research Areas (A) "Condensed Conjugation" (No. JP20H05869) from Japan Society for the Promotion of Science (JSPS), and JST SPRING (Grant No. JPMJSP2125). The computations were performed using the facilities at the Supercomputer Center, Institute for Solid State Physics, University of Tokyo.

*Corresponding author: tmisawa@issp.u-tokyo.ac.jp

[1] L. Šmejkal, A. H. MacDonald, J. Sinova, S. Nakatsuji, and T. Jungwirth, Anomalous Hall antiferromagnets, Nat. Rev. Mater. **7**, 482 (2022).
[2] L. Šmejkal, J. Sinova, and T. Jungwirth, Beyond Conventional Ferromagnetism and Antiferromagnetism: A Phase with Nonrelativistic Spin and Crystal Rotation Symmetry, Phys. Rev. X **12**, 031042 (2022).
[3] L. Šmejkal, J. Sinova, and T. Jungwirth, Emerging Research Landscape of Altermagnetism, Phys. Rev. X **12**, 040501 (2022).
[4] I. Mazin (The PRX Editors), Editorial: Altermagnetism—A New Punch Line of Fundamental Magnetism, Phys. Rev. X **12**, 040002 (2022).
[5] Y. Noda, K. Ohno, and S. Nakamura, Momentum-dependent band spin splitting in semiconducting MnO_2: a density functional calculation, Phys. Chem. Chem. Phys. **18**, 13294 (2016).
[6] M. Naka, S. Hayami, H. Kusunose, Y. Yanagi, Y. Motome, and H. Seo, Spin current generation in organic antiferromagnets, Nat. Commun. **10**, 4305 (2019).
[7] S. Hayami, Y. Yanagi, and H. Kusunose, Momentum-dependent spin splitting by collinear antiferromagnetic ordering, J. Phys. Soc. Jpn. **88**, 123702 (2019).
[8] K.-H. Ahn, A. Hariki, K.-W. Lee, and J. Kuneš, Antiferromagnetism in RuO_2 as d-wave Pomeranchuk instability, Phys. Rev. B **99**, 184432 (2019).
[9] L.-D. Yuan, Z. Wang, J.-W. Luo, E. I. Rashba, and A. Zunger, Giant momentum-dependent spin splitting in centrosymmetric low-Z antiferromagnets, Phys. Rev. B **102**, 014422 (2020).
[10] L. Šmejkal, R. González-Hernández, T. Jungwirth, and J. Sinova, Crystal time-reversal symmetry breaking and spontaneous Hall effect in collinear antiferromagnets, Sci. Adv. **6**, eaaz8809 (2020).
[11] M. Naka, S. Hayami, H. Kusunose, Y. Yanagi, Y. Motome, and H. Seo, Anomalous Hall effect in κ-type organic antiferromagnets, Phys. Rev. B **102**, 075112 (2020).
[12] M. Naka, Y. Motome, and H. Seo, Perovskite as a spin current generator, Phys. Rev. B **103**, 125114 (2021).
[13] I. I. Mazin, K. Koepernik, M. D. Johannes, R. González-Hernández, and L. Šmejkal, Prediction of unconventional magnetism in doped $FeSb_2$, Proc. Natl. Acad. Sci. U.S.A. **118**, e2108924118 (2021).
[14] Z. Feng, X. Zhou, L. Šmejkal, L. Wu, Z. Zhu, H. Guo, R. González-Hernández, X. Wang, H. Yan, P. Qin *et al.*, An anomalous Hall effect in altermagnetic ruthenium dioxide, Nat. Electron. **5**, 735 (2022).
[15] H. van Leuken and R. A. de Groot, Half-metallic antiferromagnets, Phys. Rev. Lett. **74**, 1171 (1995).
[16] W. E. Pickett, Spin-density-functional-based search for half-metallic antiferromagnets, Phys. Rev. B **57**, 10613 (1998).
[17] H. Akai and M. Ogura, Half-metallic diluted antiferromagnetic semiconductors, Phys. Rev. Lett. **97**, 026401 (2006).
[18] S. A. Egorov and R. A. Evarestov, Colossal spin splitting in the monolayer of the collinear antiferromagnet MnF_2, J. Phys. Chem. Lett. **12**, 2363 (2021).
[19] R. Stinshoff, G. H. Fecher, S. Chadov, A. K. Nayak, B. Balke, S. Ouardi, T. Nakamura, and C. Felser, Half-metallic compensated ferrimagnetism with a tunable compensation point over a wide temperature range in the Mn-Fe-V-Al Heusler system, AIP Adv. **7**, 105009 (2017).
[20] R. Stinshoff, A. K. Nayak, G. H. Fecher, B. Balke, S. Ouardi, Y. Skourski, T. Nakamura, and C. Felser,

Completely compensated ferrimagnetism and sublattice spin crossing in the half-metallic Heusler compound $Mn_{1.5}FeV_{0.5}Al$, Phys. Rev. B **95**, 060410(R) (2017).
[21] P. Midhunlal, J. A. Chelvane, D. Prabhu, R. Gopalan, and N. H. Kumar, $Mn_2V_{0.5}Co_{0.5}Z$ (Z = Ga, Al) Heusler alloys: High T_C compensated P-type ferrimagnetism in arc melted bulk and N-type ferrimagnetism in melt-spun ribbons, J. Magn. Magn. Mater. **489**, 165298 (2019).
[22] S. Semboshi, R. Y. Umetsu, Y. Kawahito, and H. Akai, A new type of half-metallic fully compensated ferrimagnet, Sci. Rep. **12**, 10687 (2022).
[23] Y. Nakano, Y. Takahashi, K. Ishida, M. Ishikawa, and H. Yamochi (private communication).
[24] See Supplemental Material at http://link.aps.org/supplemental/10.1103/PhysRevLett.132.156502 for details of parameters in the *ab initio* low-energy effective Hamiltonian, the partial density of states, the Hartree-Fock approximation, mVMC analysis of the ground-state phase diagrams, and mean-field Hamiltonian in the momentum space, which includes Refs. [26–34].
[25] Y. Nakano, Y. Takahashi, K. Ishida, M. Ishikawa, H. Yamochi, and M. Uruichi, Crystal structure and physical properties of radical cation salt based on 4, 5-ethylenedioxy-4′-iodotetrathiafulvalene (EDO-TTF-I) with iodine bonding ability, Mater. Chem. Front. **2**, 752 (2018).
[26] P. Giannozzi, O. Andreussi, T. Brumme, O. Bunau, M. B. Nardelli, M. Calandra, R. Car, C. Cavazzoni, D. Ceresoli, M. Cococcioni *et al.*, Advanced capabilities for materials modelling with Quantum ESPRESSO, J. Phys. Condens. Matter **29**, 465901 (2017).
[27] K. Nakamura, Y. Yoshimoto, Y. Nomura, T. Tadano, M. Kawamura, T. Kosugi, K. Yoshimi, T. Misawa, and Y. Motoyama, RESPACK: An *ab initio* tool for derivation of effective low-energy model of material, Comput. Phys. Commun. **261**, 107781 (2021).
[28] K. Nakamura, Y. Yoshimoto, Y. Nohara, and M. Imada, *Ab initio* low-dimensional physics opened up by dimensional downfolding: Application to LaFeAsO, J. Phys. Soc. Jpn. **79**, 123708 (2010).
[29] K. Nakamura, Y. Yoshimoto, and M. Imada, *Ab initio* two-dimensional multiband low-energy models of $EtMe_3Sb[Pd(dmit)_2]_2$ and κ-$(BEDT\text{-}TTF)_2Cu(NCS)_2$ with comparisons to single-band models, Phys. Rev. B **86**, 205117 (2012).
[30] K. Ido, K. Yoshimi, T. Misawa, and M. Imada, Unconventional dual 1D–2D quantum spin liquid revealed by *ab initio* studies on organic solids family, npj Quantum Mater. **7**, 48 (2022).
[31] D. Ohki, K. Yoshimi, A. Kobayashi, and T. Misawa, Gap opening mechanism for correlated Dirac electrons in organic compounds α-$(BEDT\text{-}TTF)_2I_3$ and α-$(BEDT\text{-}TSeF)_2I_3$, Phys. Rev. B **107**, L041108 (2023).
[32] K. Yoshimi, T. Misawa, T. Tsumuraya, and H. Seo, Comprehensive *Ab Initio* investigation of the phase diagram of quasi-one-dimensional molecular solids, Phys. Rev. Lett. **131**, 036401 (2023).
[33] T. Misawa, S. Morita, K. Yoshimi, M. Kawamura, Y. Motoyama, K. Ido, T. Ohgoe, M. Imada, and T. Kato, mVMC—Open-source software for many-variable variational Monte Carlo method, Comput. Phys. Commun. **235**, 447 (2019).
[34] https://isspns-gitlab.issp.u-tokyo.ac.jp/k-yoshimi/edottf.
[35] K. Momma and F. Izumi, VESTA3 for three-dimensional visualization of crystal, volumetric and morphology data, J. Appl. Crystallogr. **44**, 1272 (2011).
[36] D. R. Hamann, Optimized norm-conserving Vanderbilt pseudopotentials, Phys. Rev. B **88**, 085117 (2013).
[37] M. Schlipf and F. Gygi, Optimization algorithm for the generation of ONCV pseudopotentials, Comput. Phys. Commun. **196**, 36 (2015).
[38] J. P. Perdew, K. Burke, and M. Ernzerhof, Generalized gradient approximation made simple, Phys. Rev. Lett. **77**, 3865 (1996).
[39] M. Methfessel and A. T. Paxton, High-precision sampling for Brillouin-zone integration in metals, Phys. Rev. B **40**, 3616 (1989).
[40] F. Aryasetiawan, M. Imada, A. Georges, G. Kotliar, S. Biermann, and A. I. Lichtenstein, Frequency-dependent local interactions and low-energy effective models from electronic structure calculations, Phys. Rev. B **70**, 195104 (2004).
[41] M. Imada and T. Miyake, Electronic structure calculation by first principles for strongly correlated electron systems, J. Phys. Soc. Jpn. **79**, 112001 (2010).
[42] D. Tahara and M. Imada, Variational Monte Carlo method combined with quantum-number projection and multi-variable optimization, J. Phys. Soc. Jpn. **77**, 114701 (2008).
[43] M. C. Gutzwiller, Effect of correlation on the ferromagnetism of transition metals, Phys. Rev. Lett. **10**, 159 (1963).
[44] R. Jastrow, Many-body problem with strong forces, Phys. Rev. **98**, 1479 (1955).
[45] M. Capello, F. Becca, M. Fabrizio, S. Sorella, and E. Tosatti, Variational description of mott insulators, Phys. Rev. Lett. **94**, 026406 (2005).
[46] P. Ring and P. Schuck, *The Nuclear Many-Body Problem* (Springer Science & Business Media, New York, 2004).
[47] T. Mizusaki and M. Imada, Quantum-number projection in the path-integral renormalization group method, Phys. Rev. B **69**, 125110 (2004).
[48] F. Becca and S. Sorella, *Quantum Monte Carlo Approaches for Correlated Systems* (Cambridge University Press, Cambridge, England, 2017).
[49] S. Sorella, Generalized Lanczos algorithm for variational quantum Monte Carlo, Phys. Rev. B **64**, 024512 (2001).
[50] I. I. Mazin, Notes on altermagnetism and superconductivity, arXiv:2203.05000.